AMERICAN SOCIETY FOR MICROBIOLOGY | Journal of Virology®

STRUCTURE AND ASSEMBLY

Structural Study of the C-Terminal Domain of Nonstructural Protein 1 from Japanese Encephalitis Virus

Thanalai Poonsiri,[a,c] Gareth S. A. Wright,[a] Michael S. Diamond,[d,e,f] Lance Turtle,[b,c] Tom Solomon,[c] Svetlana V. Antonyuk[a]

[a]Molecular Biophysics Group, Institute of Integrative Biology, Faculty of Health and Life Sciences, University of Liverpool, Liverpool, United Kingdom

[b]Centre for Global Vaccine Research, Institute of Infection and Global Health, University of Liverpool, Liverpool, United Kingdom

[c]Health Protection Research Unit on Emerging and Zoonotic Infections, Institute of Infection and Global Health, University of Liverpool, Liverpool, United Kingdom

[d]Department of Medicine, Washington University School of Medicine in St. Louis, St. Louis, Missouri, USA

[e]Department of Molecular Microbiology, Washington University School of Medicine in St. Louis, St. Louis, Missouri, USA

[f]Department of Pathology & Immunology, Washington University School of Medicine in St. Louis, St. Louis, Missouri, USA

ABSTRACT Japanese encephalitis virus (JEV) is a mosquito-transmitted flavivirus that is closely related to other emerging viral pathogens, including dengue virus (DENV), West Nile virus (WNV), and Zika virus (ZIKV). JEV infection can result in meningitis and encephalitis, which in severe cases cause permanent brain damage and death. JEV occurs predominantly in rural areas throughout Southeast Asia, the Pacific Islands, and the Far East, causing around 68,000 cases of infection worldwide each year. In this report, we present a 2.1-Å-resolution crystal structure of the C-terminal β-ladder domain of JEV nonstructural protein 1 (NS1-C). The surface charge distribution of JEV NS1-C is similar to those of WNV and ZIKV but differs from that of DENV. Analysis of the JEV NS1-C structure, with *in silico* molecular dynamics simulation and experimental solution small-angle X-ray scattering, indicates extensive loop flexibility on the exterior of the protein. This, together with the surface charge distribution, indicates that flexibility influences the protein-protein interactions that govern pathogenicity. These factors also affect the interaction of NS1 with the 22NS1 monoclonal antibody, which is protective against West Nile virus infection. Liposome and heparin binding assays indicate that only the N-terminal region of NS1 mediates interaction with membranes and that sulfate binding sites common to NS1 structures are not glycosaminoglycan binding interfaces. This report highlights several differences between flavivirus NS1 proteins and contributes to our understanding of their structure-pathogenic function relationships.

IMPORTANCE JEV is a major cause of viral encephalitis in Asia. Despite extensive vaccination, epidemics still occur. Nonstructural protein 1 (NS1) plays a role in viral replication, and, because it is secreted, it can exhibit a wide range of interactions with host proteins. NS1 sequence and protein folds are conserved within the *Flavivirus* genus, but variations in NS1 protein-protein interactions among viruses likely contribute to differences in pathogenesis. Here, we compared characteristics of the C-terminal β-ladder domain of NS1 between flaviviruses, including surface charge, loop flexibility, epitope cross-reactivity, membrane adherence, and glycosaminoglycan binding. These structural features are central to NS1 functionality and may provide insight into the development of diagnostic tests and therapeutics.

Received 26 October 2017 **Accepted** 12 January 2018

Accepted manuscript posted online 17 January 2018

Citation Poonsiri T, Wright GSA, Diamond MS, Turtle L, Solomon T, Antonyuk SV. 2018. Structural study of the C-terminal domain of nonstructural protein 1 from Japanese encephalitis virus. J Virol 92:e01868-17. https://doi.org/10.1128/JVI.01868-17.

Editor Julie K. Pfeiffer, University of Texas Southwestern Medical Center

Address correspondence to Svetlana V. Antonyuk, S.Antonyuk@liverpool.ac.uk.

KEYWORDS Japanese encephalitis virus, protein crystallography, neutralizing antibodies, nonstructural protein 1, protein structure-function

Japanese encephalitis virus (JEV) is a positive-sense single-stranded RNA virus with a 10.9-kb genome which is translated into a polyprotein consisting of three structural proteins (capsid, membrane, and envelope protein [E]) and seven nonstructural proteins, including nonstructural protein 1 (NS1), NS2A, NS2B, NS3, NS4, NS4B, and NS5. Flavivirus NS1 is a multifunctional glycoprotein that has drawn attention because of its importance in viral replication, immune modulation, and immune evasion. Mutagenesis and transcomplementation assays have established that flavivirus NS1 is essential for RNA replication (1–5) and colocalizes with the replication complex (2). Transcomplementation suppressor mutagenesis studies indicate that yellow fever virus (YFV) NS1 interacts with NS4A (6) and that West Nile virus (WNV) NS1 interacts with NS4B (7). WNV NS1 forms a physical complex with NS4B based on coimmunoprecipitation experiments (7). NS1 has been described as a complement-fixing antigen (8–11), and dengue virus (DENV) NS1 binds to complement pathway components C1s, C4, and C4b (12, 13), whereas WNV NS1 can also interact with factor H (14) for protection of infected cells from complement-dependent clearance. NS1 may also interfere with the double-stranded RNA (dsRNA) sensor Toll-like receptor 3 (TLR-3) (15) to escape host pathogen recognition receptor detection. DENV NS1 can induce inflammatory cytokine production, endothelial cell permeability, and changes to the glycocalyx (16), possibly through interactions with TLR-4; all of those activities appear to contribute to the development of severe dengue (17, 18). Although direct interactions between JEV NS1 and TLR-4 have not been evaluated, it may play a role in JEV pathogenesis, because deletion of the TLR-4 gene enhances resistance to JEV (19).

A signal sequence at the C terminus of E protein translocates NS1 to the endoplasmic reticulum (ER), where it undergoes cleavage and posttranslational modification (20). There are two characterized forms of NS1: a membrane-associated dimer (~49 kDa per monomer), found on ER surface and the plasma membrane, and a secreted hexamer (52 to 55 kDa per monomer) (20). The masses of the two NS1 forms are different due to differential glycosylation. Structures of full-length NS1 proteins of WNV (21, 22), DENV (22), and ZIKV (23, 24) have been reported. Most NS1 proteins contain six conserved disulfide bonds. The NS1 forms share a conserved N-linked glycosylation site at Asn 207. YFV, DENV, WNV, and JEV share a second glycosylation site at Asn 130, and most of the JEV serogroup NS1 proteins have a third glycosylation site at Asn175 linked to high-mannose carbohydrate, but it is not present in JEV NS1 itself (20, 25–27). The NS1 monomer of WNV, DENV, and ZIKV contains 3 domains: the β-roll (amino acid residues 1 to 29), wing (38 to 151), and β-ladder (181 to 352) domains (22–24). NS1 forms a homodimer by extending the β-ladder domain and connecting at the β-roll domain, forming a cross-shaped protein. One face of the dimer comprises the protruding β-roll domain and part of the wing domain. The hydrophobic surface of the β-roll and wing domains may mediate the interaction with the cell membrane (22) via a number of amino acid residues identified in ZIKV, including amino acid residues 28, 115, 118, 123, and 160 to 163 (23, 24). The opposite side is composed of loops linking the surface β-strands of the ladder domain. This region is a potential host protein interacting surface due to its hydrophilicity. Three NS1 dimers can assemble to form a hexameric pore, which can act as a lipid depot (22, 28). DENV NS1 expression on the infected cell surface may occur via a glycosylphosphatidylinositol (GPI) anchor, for which a hydrophobic carboxy-terminal GPI addition signal peptide at the N terminus of NS2A is required (29–31). Soluble NS1 also binds to uninfected cell membranes via glycosaminoglycans (GAGs), primarily heparan sulfate and chondroitin sulfate E (32).

Secreted NS1 is used as a diagnostic marker for flavivirus infection, as it is found in the blood at early stages (33, 34). Alternatively, detection of anti-NS1 IgM and IgG can be used (34, 35). Immunization of NS1 in mice or passive transfer of anti-NS1 antibodies (Abs) can confer protective effects against flavivirus challenge (34, 36–39). However,

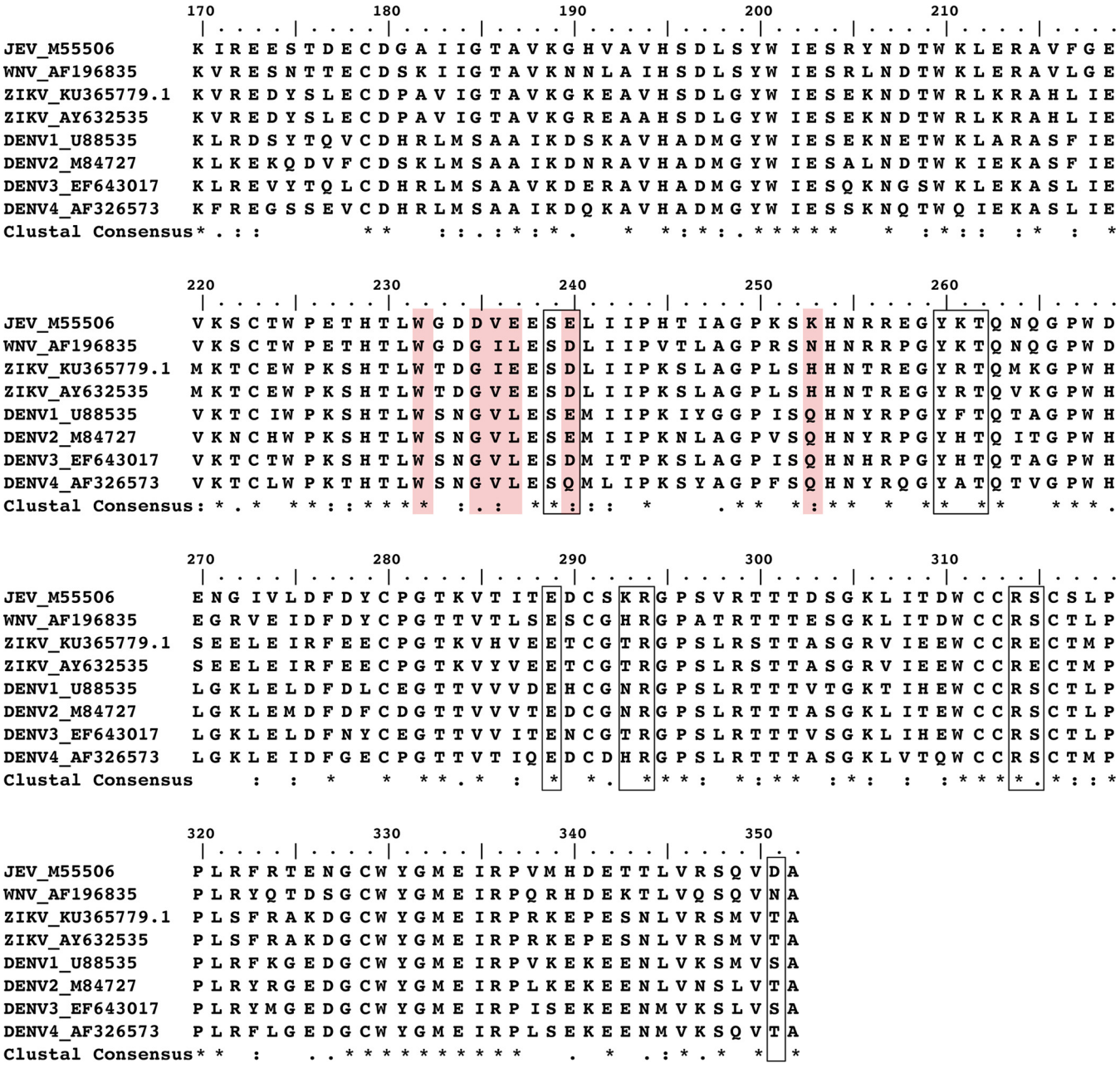

FIG 1 Sequence alignment of full-length flavivirus NS1 produced from Clustal W (1). An asterisk indicates a fully conserved residue. A colon indicates conservation between groups of strongly similar properties. A period indicates conservation between groups of weakly similar properties. The following amino acid sequences were used for X-ray structure studies: DENV1 U88535 for PDB ID 4OIG; DENV2 M84727 for PDB ID 4O6B; WNV 196835 for PDB ID 4O6C and PDB ID 4OIE; ZIKV KU365779 for PDB ID 5IY3; and ZIKV AY632535 for PDB ID 5K6K and PDB ID 5GS6. The 22NS1 light-chain epitopes are highlighted in red, and heavy-chain epitopes are in black rectangles.

some anti-DENV NS1 antibodies reportedly are autoreactive and bind to host extracellular matrix components, platelets, and endothelial cells (8, 20), which may have pathogenic consequences. Flavivirus NS1 transferred with blood meal was found to enhance viral infection in mosquitoes by downregulating mosquito midgut immune genes (40).

Most of our knowledge of JEV NS1 has been inferred from studies of DENV and WNV NS1. Although the protein sequences are highly conserved (Fig. 1) and the DENV, WNV, and ZIKV NS1 structures display the same protein fold, there are important differences. For example, polyclonal antibodies raised against DENV NS1 in mice were shown to

cross-react with proteins on epithelial cells: ATPase, protein disulfide isomerase, vimentin, and heat shock protein 60. The cross-reactive epitope was mapped to amino acid residues 311 to 330 on DENV NS1 (41) (Fig. 1). Although JEV NS1 shares these conserved epitopes, antibodies against JEV NS1 did not react to any of these host cell targets (41). NS1 alone was shown to cause endothelial leakage in DENV, but this was not detected in WNV, consistent with the non-vascular-leakage phenotype of WNV disease (42). Similarly to WNV, other encephalitic flaviviruses, including JEV, may vary in their NS1-endothelium interactions. As another example, WNV NS1 binds the alternative complement pathway regulator factor H, whereas JEV NS1 does not (8).

NS1′ is an extended form of NS1 with 52 extra amino acids from the NS2A N terminus, generated by a −1 ribosomal frameshift (43). It is specific to the JE serogroup of flaviviruses. NS1′ was found in dimeric form (monomer molecular mass of around 58 kDa), has been detected in both cell lysate and culture media (44, 45), and has been suggested to play a role in neuroinvasiveness; selectively abolishing NS1′ production reduces WNV mortality in mice (43, 46). NS1′ colocalized with viral RNA replication complex and can substitute for NS1 in cells (45). However, there is a discrepancy between the results of *in vitro* and those of *in vivo* studies. WNV NS1′ provides an advantage only in *in vivo* studies (47). There is also variation with respect to NS1′ involvement in replication among different viruses. Whereas WNV NS1′ does not contribute to viral replication *in vitro*, JEV NS1′ mutants have less infectivity in a cell model (47, 48). Therefore, the role of NS1′ in JEV life cycle and pathogenesis remains unclear.

Here, we report the crystal structure of the C-terminal domain (amino acids 172 to 352) of JEV NS1 and compare it with published DENV, WNV, and ZIKV NS1 structures. Our findings reveal diversity in protein surface charges. Furthermore, the solution conformation of the protein was examined by small-angle X-ray scattering (SAXS) and molecular dynamics (MD) simulations along with analysis of cell membrane association. Importantly, we define a cross-reactive epitope on NS1 using an antibody that shows protective activity against WNV infection. Our study results show the common and contrasting features of flavivirus NS1 structures and contribute to our knowledge of the molecular basis of multiple NS1 functions.

RESULTS

Structure of C-terminal domain of JEV NS1 and NS1′. The crystal structure of the C-terminal region of JEV NS1 determined at 2.1-Å resolution is similar to all previously solved flavivirus NS1 structures with respect to fold characteristics (Fig. 2a). The electron density is visible for residues 177 to 352, whereas that of the first 5 residues at the N terminus is not visible. The monomer consists of 10 β-strands on one side and 4 helices and unstructured loops on the other side. Between the β-strands in each pair are β-turns and short loops, apart from β4 and β5, which are separated by a long unstructured loop (residues 218 to 273) (Fig. 2a and b). The protein contains four conserved disulfide bonds (C179—C229, C280—C329, C291—C312, and C313—C316) and hydrogen bonds between β-strands and loops. JEV NS1-C forms 20 β-strands oriented in a head-to-head arrangement in the dimer, as do ZIKV, WNV, and DENV NS1, with a dimer length of 9.65 nm at its widest point (Fig. 2c). The dimer interface is created by 21 residues from each monomer, with an average distance of 2.9 Å (Tables 1 and 2). Eight of these interface residues are conserved among flavivirus NS1 proteins (Table 1, scores 7 to 9). The dimer is connected by 12 hydrogen bonds. Comparing the hydrogen bonding networks at the dimer interface of the C-terminal domains of ZIKV (PDB identifier [ID] 5IY3), WNV (PDB ID 4OIE), and DENV NS1 (PDB ID 4OIG), there are 6 common residues with the same bond arrangement: Thr (JEV, ZIKV, WNV)/Ala (DENV) 186, Val (JEV, ZIKV, WNV)/Ile (DENV) 188, Thr (JEV, WNV)/Ser (ZIKV, DENV) 228, His 254, and Thr 230 to Trp 232 (Tables 1, 2, and 3) (Fig. 3). In addition, we solved the structure of JEV NS1′-C, which is distinguished from NS1 by the presence of an extra 52 amino acids at the C terminus of the protein, to 2.6-Å resolution. The structure revealed the same protein fold and dimer orientation. However, it showed only 2 extra amino acids

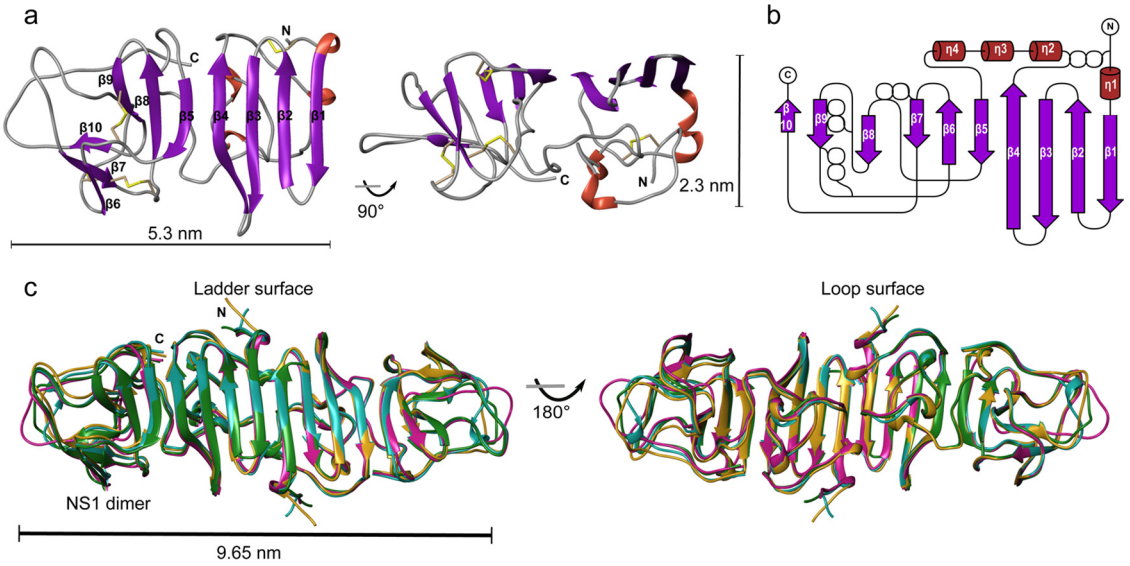

FIG 2 The C-terminal domain structure of JEV NS1. (a) Ribbon model of JEV NS1-C monomer. One side is built of 10 β-strands, and the opposite side consists of the nonstructured loops. Disulfide bonds are shown in yellow. (b) Topology diagram of JEV NS1-C. Four disulfide bonds are indicated as white spheres. "β" represents the β-sheet, and "η" represents the 310 helix. (c) Superimposed ribbon diagram of NS1-C of JEV (magenta), ZIKV (PDB ID 5IY3, blue), WNV (PDB ID 4OIE, green), and DENV1 (PDB ID 4OIG, gold).

in comparison with the C-terminal domain of JEV NS1 (0.348-Å Cα root mean square deviation [RMSD]) (data not shown). The C terminus is disordered, so the electron density is not visible.

Solution model of JEV NS1-C dimer. The dimeric nature of JEV NS1-C was confirmed by SAXS studies performed on the protein in solution. The SAXS profiles calculated from the monomer and dimer of JEV NS1-C crystal structure were compared with the JEV NS1-C experimental SAXS data (Fig. 4a). A monomer of JEV NS1-C yielded a poor fit to the experimental data with χ of 14.11, whereas a dimer provided an improved fit with χ of 4.02. A radius of gyration of 27.02 Å was obtained from Guinier

TABLE 1 JEV NS1 C-terminal dimer interfacing residues

No.	Residue	ASA (Å^2)[a]	BSA (Å^2)[b]	ΔG (kcal/mol)[c]	Conservation[d]
1	Gly181	23.56	6.81	0.03	3
2	Ala182	91.29	45.68	0.30	1
3	Ile184	22.47	16.36	−0.18	5
4	Gly185	40.33	16.05	0.26	7
5	Thr186	37.46	36.73	−0.22	7
6	Ala187	63.58	21.49	0.34	9
7	Val188	64.98	63.40	0.34	6
8	Lys189	181.59	9.98	0.16	8
9	Gly190	63.17	54.83	0.30	5
10	His191	110.70	33.66	0.74	1
11	Trp210	60.01	29.42	0.08	5
12	Glu227	104.51	54.79	0.51	5
13	Thr228	120.12	94.74	0.66	6
14	His229	54.08	52.04	0.90	9
15	Thr230	24.89	21.26	−0.20	9
16	Leu231	48.09	48.09	0.77	8
17	Trp232	95.68	59.18	0.38	5
18	Gly233	39.95	30.60	−0.02	4
19	Asp234	91.67	54.93	0.26	6
20	Asp235	128.72	0.58	−0.01	1
21	His254	13.56	10.75	0.73	8

[a]ASA, accessible surface area (determined by assembly analysis in the program PISA).
[b]BSA, buried surface area (determined by assembly analysis in the program PISA).
[c]ΔG, solvation energy effect (determined by assembly analysis in the program PISA).
[d]Amino acid conservation values represent Consurf scores (9, conserved; 1, variable).

TABLE 2 Hydrogen bonds between JEV NS1 C-terminal dimer interfacing residues

No.	Structure 1	Distance (Å)[a]	Structure 2
1	Gly190 [N]	2.93	Ile184 [O]
2	Val188 [N]	2.86	Thr186 [O]
3	Thr186 [N]	2.89	Val188 [O]
4	His229 [NE2]	2.83	Gly190 [O]
5	His254 [NE2]	2.94	Thr228 [O]
6	Trp232 [N]	2.96	Thr230 [O]
7	Ile184 [O]	2.93	Gly190 [N]
8	Thr186 [O]	2.86	Val188 [N]
9	Val188 [O]	2.89	Thr186 [N]
10	Gly190 [O]	2.83	His229 [NE2]
11	Thr228 [O]	2.94	His254 [NE2]
12	Thr230 [O]	2.96	Trp232 [N]

[a]Data represent results of assembly analysis in the program PISA.

analysis, and that value is consistent with the value extracted from the pair distribution function, 27.08 Å. The pair distribution function of JEV NS1-C shows characteristics of a lengthy ovoid particle with a maximum intraparticle distance (D_{max}) of 94.1 Å, similar to the widest point of JEV NS1-C dimer crystal structure (96.5 Å) (Fig. 2c and 4b). The calculated molecular mass was 45.5 kDa, corresponding to the dimeric form of C terminus NS1. An averaged *ab initio* model was generated at 30-Å resolution with good similarity agreement (normal spatial discrepancy [NSD] = 0.513 ± 0.016) and was compared with the JEV NS1-C dimer crystal structure (Fig. 4c). The structures were well matched, although there was an extra region of mass near the dimer interface in the SAXS model (labeled M; Fig. 4c). This feature also is seen in the SAXS model of WNV, suggesting that the NS1 crystal structures of JEV and WNV may not fully represent the structure of the protein in solution (21). Analysis of the crystallographic atomic mean square displacements or B-factors in our JEV NS1-C crystal structure indicates that surface regions of loop 218 to 272, particularly subloop 235 to 237, had high conformational freedom within the crystal lattice (Fig. 4d and e). A 40-ns all-atom molecular dynamics (MD) simulation of the JEV NS1-C dimer at 37°C confirmed that the movement of this loop was unrestrained in both monomers (Fig. 4d and e). We hypothesized that the apparent extra region of mass observed in the JEV NS1-C and WNV SAXS structures could be accounted for by the dynamic nature of loop 218 to 272 and the resulting expansion of volume in the solution structures. To model JEV NS1-C behavior in solution more accurately, we created a pool of possible structures with various conformations of loop 218 to 272 and compared them with our SAXS data. Using this approach, we improved the fit to the experimental SAXS data from χ of 4.02 to χ of 1.48 (Fig. 4a).

Comparison of JEV NS1-C with other flavivirus NS1-C structures. JEV NS1-C has the same fold characteristics as ZIKV (2.2-Å resolution), WNV (2.6-Å resolution), and DENV (3-Å resolution) NS1-C, and superposition gives Cα RMSD values closest to that determined for WNV NS1 (1.162 Å for ZIKV, 0.959 Å for WNV, and 1.333 Å for DENV) (Fig. 2c). The structural superimposition showed low positional conservation only at the N terminus, C terminus, and β-turns. The electrostatic surface potential maps of known NS1-C domains (ZIKV, WNV, and DENV) showed symmetric patterns consistent with homodimers. On the β-ladder surface, all displayed a neutral charge in the central regions flanked by negatively charged regions (Fig. 5). This negatively charged region is small in DENV and larger in WNV and can be seen to expand diagonally from the top left to bottom right in JEV and ZIKV in the figure. Adjacent to it, toward the ends, are small positively charged pockets that are seen clearly only in JEV and ZIKV, and the tips of all NS1-C proteins have mixed charges. The loop surface is more variable than the ladder surface. DENV has a distinct positively charged central region, whereas JEV and WNV have a negative charge in their central area. ZIKV is different, as the middle region displays both positive and negative charges. The adjacent area has positively charged pockets in all NS1 structures (Fig. 5 and Table 4). Three pockets are found in WNV and

TABLE 3 Residues forming a hydrogen bond at a dimer interface compared with existing flavivirus NS1[a]

	ZIKV residue			WNV residue			DENV residue	
JEV residue	5K6K	5GS6	5IY3	4O6D	4O6C	4OIE	4O6B	4OIG
	Asp1	His1		Asp1	Asp1			
	Val2	**Val2**		**Thr2**	**Thr2**		**Ser2**	
	Cys4	**Cys4**		**Cys4**	**Cys4**		**Cys4**	
	Ser5	**Ser5**						
	Val6	**Val6**		**Ile6**	**Val6**		**Ile6**	
	Phe8							
	Ser9							
				Arg10	Arg10			
	Lys11							
	Glu12			Glu12	Glu12			
				Leu13				
	Arg14	**Arg14**		**Arg14**	**Arg14**		**Lys14**	
	Thr17	**Thr17**		**Ser17**	**Ser17**		**Ser17**	
	Val19	**Val19**		**Val19**	**Val19**		**Ile19**	
	Phe20	Phe20		Phe20	Phe20			
	Ile21	**Val21**		**Ile21**	**Ile21**		**Ile21**	
	Tyr22	Tyr22						
	Asn23	**Asn23**		**Asn23**	**Asn23**		**Asp23**	
	Asp24	Asp24		Asp24	Asp24			
	Arg31			Arg31	Arg31			
	Tyr32			Tyr32	Tyr32			
	Asp157	Asp157						
							Tyr158	
				Phe160				
	Thr165			Thr165	Thr165			
				Ser181	Ser181			
				Lys182	Lys182			Arg182
Ile184	Ile184	Ile184	Ile184					
								Ser185
Thr186	**Thr186**	**Thr186**	**Thr186**	**Thr186**	**Thr186**	**Thr186**	**Ala186**	**Ala186**
Val188	**Val188**	**Val188**	**Val188**	**Val188**	**Val188**	**Val188**	**Ile188**	**Ile188**
	Lys189			Lys189	Lys189			Lys189
Gly190	Gly190	Gly190	Gly190					Asp190
		Lys191		Asn191	Asn191			
	192Glu	Glu192						
	193Ala							
	Glu203			Glu203				
	Lys227	Lys227	Lys227					
Thr228	**Ser228**	**Ser228**	**Ser228**	**Thr228**	**Thr228**	**Thr228**	**Ser228**	**Ser228**
His229	His229	His229	His229					
Thr230	**Thr230**	**Thr230**	**Thr230**	**Thr230**	**Thr230**	**Thr230**	**Thr230**	**Thr230**
Trp232	**Trp232**	**Trp232**	**Trp232**	**Trp232**	**Trp232**	**Trp232**	**Trp232**	**Trp232**
	Thr233	Thr233	Thr233				Ser233	Ser233
	Asp234	Asp234	Asp234				Asn234	Asn234
His254	**His254**	**His254**	**His254**	**His254**	**His254**	**His254**	**His254**	**His254**

[a]Shared residues are indicated in boldface.

DENV, whereas ZIKV has only pockets 1 and 2 and JEV has pockets 1 and 3. The residues building the positively charged pockets are conserved in pocket 1 and partially conserved in pocket 2, pocket 3, and the front pocket on the ladder surface (Fig. 5b and Table 4).

Cell membrane interaction via determination of GAGs. Sulfate molecules were found on the surface of JEV NS1-C (Fig. 6 and Table 5) that were similar to those seen with ZIKV (PDB ID 5K6K), WNV (PDB ID 4O6C), and DENV (PDB ID 4OIG). Moreover, they were found to be distributed near the positively charged pockets. Hence, it is possible that this positively charged area is the binding site of negatively charged ligands. Sulfate-containing molecules, such as GAGs, which are involved in NS1-dependent membrane attachment (32) could interact here. To test if the interaction with GAGs occurs via sulfate binding sites at the C terminus, JEV NS1-C binding to heparin agarose beads was analyzed. However, the 20-kDa JEV NS1-C was found only in the flowthrough

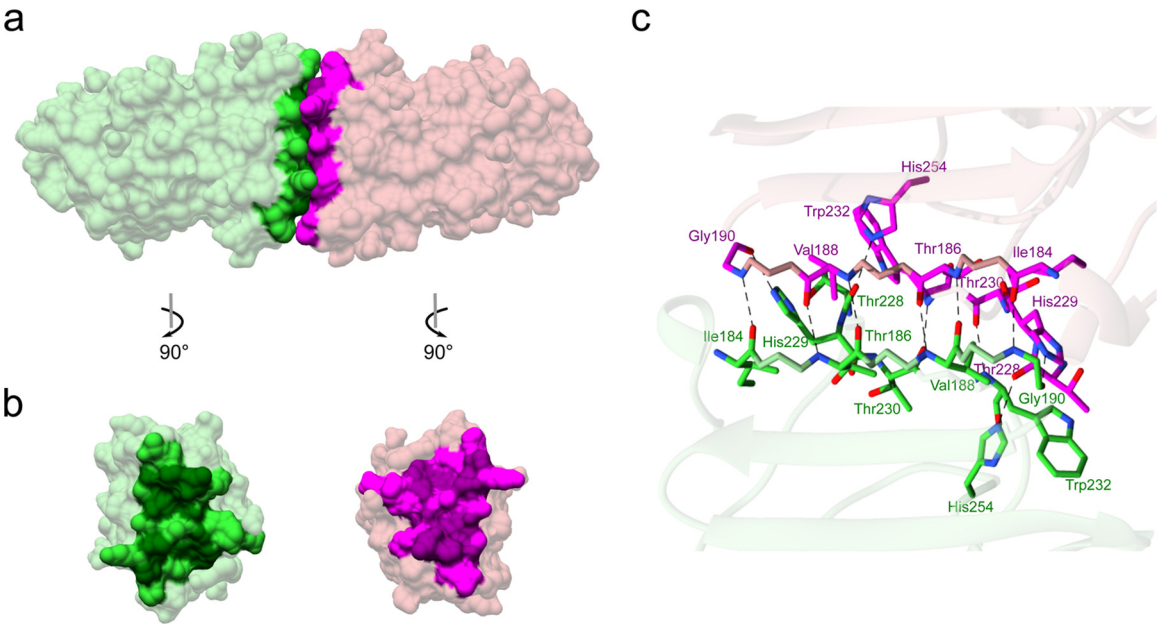

FIG 3 Dimer interface of JEV NS1-C. (a and b) The surfaces of 21 residues from one monomer involved in dimer interface are colored in lime green, and the surfaces that form hydrogen bonds are colored in dark green (a). Similarly, another monomer-interfacing surface is in magenta and surfaces forming hydrogen bonds are in dark magenta (b). (c) Residues involved in hydrogen formation at the dimer interface are highlighted in lime green and magenta as described for panels a and b. Hydrogen bonds are indicated by dashed lines.

and wash fractions (Fig. 7a), indicating that it did not interact efficiently with heparin. The interaction of heparan sulfate, chondroitin sulfate, and dermatan sulfate polymers with JEV NS1-C was investigated by protein thermal shift assay. No JEV NS1-C stabilizing effect was observed for any of GAG polymers tested even at a high concentration of GAG (100 μM). The absence of GAG binding was consistent with the results of the pulldown experiments.

Interactions of JEV NS1-C with lipids common to cell membranes were tested using a liposome binding assay. JEV NS1-C did not associate with liposomes at either pH 7.5 or pH 5.5 (Fig. 7b). As full-length NS1 can bind liposomes (22, 49), it appears that the NS1 C terminus is not responsible for membrane binding. We note that the hydrophobic residues of β-roll and wing domains have been suggested to play a role in membrane binding (22–24).

JEV NS1-C and JEV NS1′-C complexed with 22NS1 fragment antigen binding (Fab). Comparison of the 22NS1 antibody epitope of WNV-NS1-C with that of JEV NS1-C showed that 9 of 16 residues (Trp232, Ser239, Tyr260, Lys261, Thr262, Glu289, Arg294, Arg314, and Ser315) are conserved between the two viruses (Fig. 1) (36). Indeed, 22NS1 monoclonal antibody (MAb) cross-reacts with JEV NS1-C protein and NS1′-C protein, which was confirmed by Western blotting (Fig. 8, lower left inset) and size exclusion chromatography (SEC) (Fig. 8). JEV NS1-C and 22NS1 Fab alone eluted at retention times of 7.9 and 8.3 min, respectively. JEV NS1-C incubated with 22NS1 Fab eluted faster at a retention time of 6.9 min, corresponding to complex formation with a small amount of free 22NS1 Fab fragments left. The eluted fraction was analyzed by SDS-PAGE, and 2 peaks representing JEV NS1-C and 22NS1 (~25 kDa) were identified. This confirms that NS1 and 22NS1 MAb interact in solution (Fig. 8, lower right inset). The incubation also generated a small peak at a retention time of 6.1 min. This may represent a higher-order oligomer of JEV NS1-C, which recruits multiple 22NS1 monomers into a complex with a higher hydrodynamic radius than the 2:2 complex observed at 6.9 min. In support of this idea, we note the absence of the NS1-C species eluting at ~7.4 min in the complex chromatogram. The protein-Fab complex was also analyzed by SAXS. The complex experimental profile was compared to that of the WNV NS1-C–22NS1 complex (PDB ID 4OII) using the calculated SAXS profile (Fig. 9a and c). However,

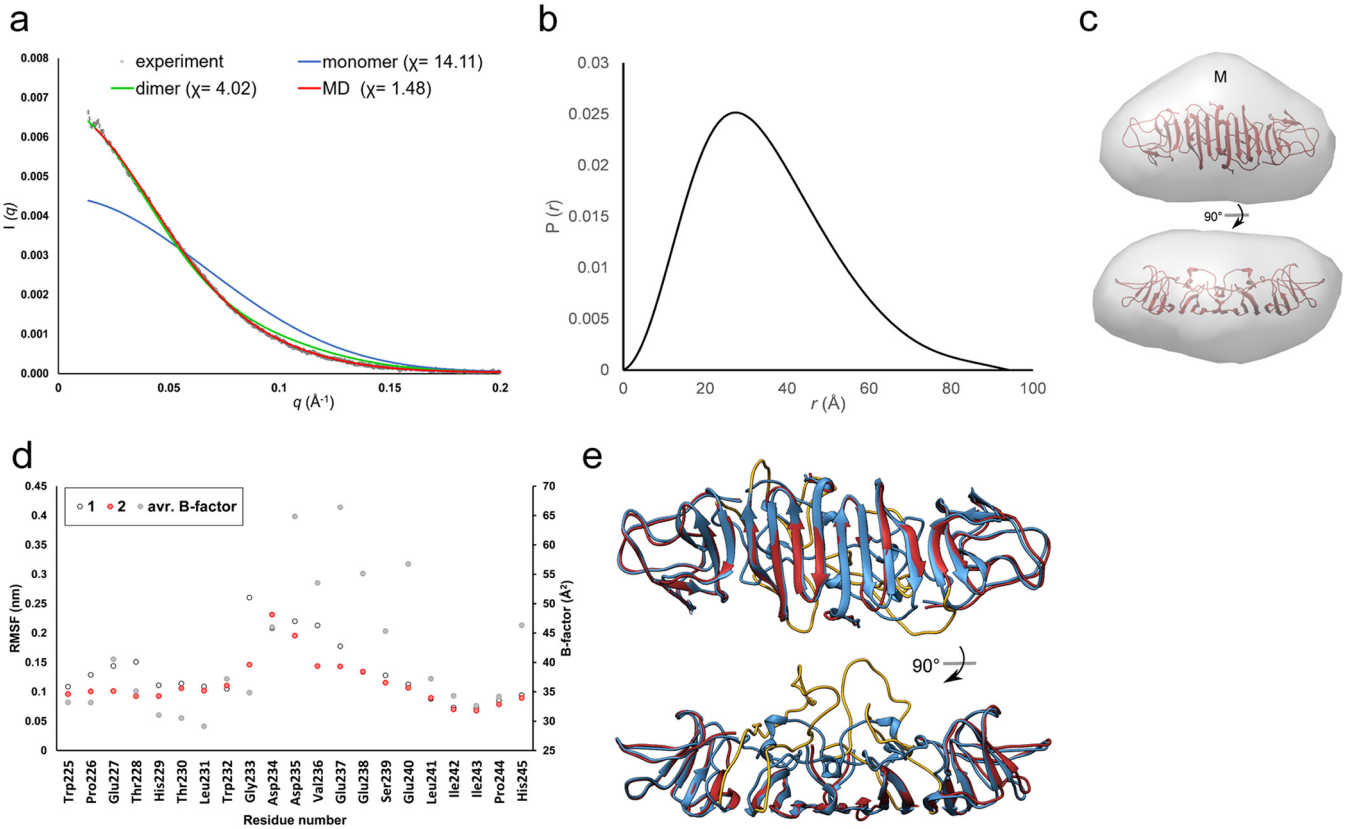

FIG 4 Solution model of JEV NS1-C dimer. (a) SAXS curve. An experimental scattering curve is shown in black scattering. Scattering profiles of JEV NS1-C monomer and dimer and the best molecular dynamic simulation structure calculated with FoXS are shown in blue, green, and red, respectively. (b) Pair distribution functions. (c) Low-resolution model of JEV NS1-C calculated from SAXS profiles docked with the crystal structure of the JEV NS1-C dimer. An extra region of mass is labeled with an "M." (d) RMSF plot of the molecular dynamic simulation at the flexible loop. RMSF values of each monomer are indicated in black and red. The average (avr.) β-factor value for each residue is indicated in gray. (e) The best molecular dynamic simulation structure (red) was superimposed with the JEV NS1-C crystal structure (blue). The flexible loop consisting of residues 218 to 272 is shown in yellow.

the complex (PDB ID 4OII) gave a poor fit to the experimental SAXS data, with a χ value of 6.82. Guinier analysis gave a radius of gyration of 52.89 $\pm$ 0.34 Å, which coincides with the 52.50-Å value extracted from the pair distribution function. The pair distribution function of the complex had multiple peaks which signify the multidomain geometric shape, with a D_{max} value of 154.9 Å (Fig. 9b). The calculated molecular mass was 149.96 kDa. An averaged *ab initio* model was generated at 30-Å resolution. The Fab part of the WNV complex (PDB ID 4OII) did not fit into the SAXS envelope and shifted from the positions in the 4OII model, whereas the WNV NS1-C dimer fit well (Fig. 9c to e), indicating flexibility of the Fab epitope in solution. We generated a pseudoatomic model of the JEV NS1-C antibody complex by replacing the WNV-NS1-C with JEV NS1-C and optimizing the position of the Fab molecules. This model, with the 2 Fab molecules shifted away from the primary location in the 4OII model, had a better fit to the SAXS data (χ of 6.82 to 3.09; Fig. 9a and c to e). Both JEV NS1-C and NS1′-C were able to cross-interact with the protective WNV 22NS1 MAb, and JEV NS1-C interacted with some flexibility.

DISCUSSION

Flavivirus NS1 proteins have generated much interest because of their multiple functions in viral replication, cell signaling, and immune evasion. Since 2014, the structures of nine NS1 proteins have been solved (21–24, 50). These proteins were expressed in bacterial or insect cell expression systems. Here, we expressed the JEV NS1 C terminus in *Escherichia coli* after the failure of several attempts to express full-length JEV NS1 in *E. coli*, insect cells, and mammalian cells. We describe the first structure of

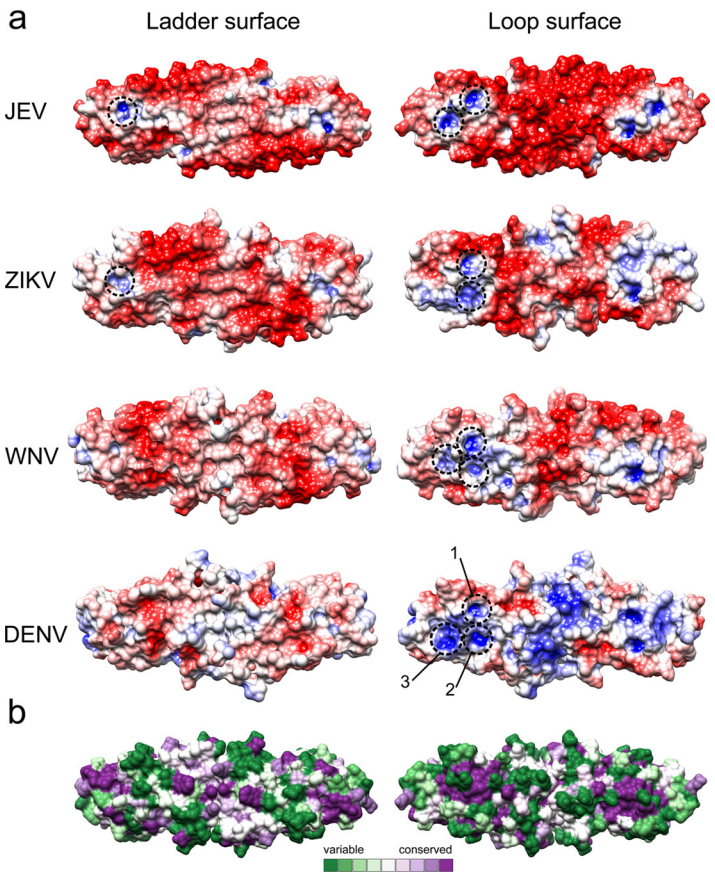

FIG 5 JEV NS1-C structure compared to other flavivirus NS1-C structures. (a) Electrostatic surface map of NS1-C structures from JEV, ZIKV, WNV, and DENV. The surface is colored according to electrostatic potential values from −5 kT/e (red) to 5 kT/e (blue). Positive potential pockets are depicted in dashed circles. (b) Surface model color coded by conservation. The most conserved residues are represented in dark magenta, and the most variable residues are represented in dark green.

the *E. coli*-expressed JEV NS1 C terminus, which, compared to other NS1 structures as well as that of JEV NS1′-C, shows a high degree of structural conservation. As expected for NS1′, the presence of the same fold could explain the similar functions of NS1 and NS1′ seen *in vitro*. However, the specific role of the extra amino acids is not yet clear, although WNV lacking the NS1′ form is less neuroinvasive (43).

The availability of WNV, DENV, and ZIKV NS1 structures has allowed us to assess similarities and differences which may be relevant to their functional behavior. All NS1 proteins are dimeric *in crystallo*, even though the recombinant protein contains only the C-terminal domain (21, 23). The molecular mass and the low-resolution model generated from SAXS data confirm the dimeric nature of the isolated C-terminal domain in solution. In contrast to previous work, which suggested that the β-roll domain is responsible for dimerization (49), we propose that 6 common residues which form hydrogen bonds at the dimer interface of all NS1 structures mediate dimer formation (49). In principle, inhibition of dimer formation by interposition of a ligand at this site could facilitate antiflavivirus drug development.

Both faces of the JEV NS1-C dimer display electrostatic surface charge diversity. However, considering the full-length flavivirus NS1 protein structure (22–24), the ladder face of the C-terminal domain is positioned under the β-roll domain (Fig. 10). The N terminus protects the central region of the ladder face from the environment. In addition, the β-roll domain is contained by a hydrophobic region that is suspected to interact with the cell membrane or to form a lipid cargo pore in NS1 hexamer, making it harder for the ladder face to interact. This model conflicts with a previous suggestion

TABLE 4 Residues forming positively charged pockets compared with existing C-NS1

JEV residue	ZIKV residue (5IY3)	WNV residue (4OIE)	DENV residue (4OIG)	Conservation[a]
Pocket 1				
Gly259	Gly259	Gly259	Gly259	9
Tyr260	Tyr260	Tyr260	Tyr260	9
Lys261	Arg261	Lys261	Phe261	1
			Ala265	1
Ser292	Gly292	Gly292	Gly292	1
Lys293	Thr293	His293	Asn293	1
Arg294	Arg294	Arg294	Arg294	9
Cys313				9
Arg314	Arg314	Arg314	Arg314	9
Ser315	Glu315	Ser315	Ser315	5
Cys316	Cys316	Cys316	Cys316	9
Glu334	Glu334	Glu334	Glu334	9
Pocket 2				
	Thr262	Thr262	Thr262	6
	Met264	Asn264	Thr264	1
	Lys265			1
	Gly295	Gly295	Gly295	9
	Pro296	Pro296	Pro296	4
		Gly332		6
	Met333	Met333	Met333	9
	Thr351	Asn351	Ser351	3
Pocket 3				
Gly295				9
Pro296				4
Ser297		Ala297	Ser297	9
Val298		Thr298	Leu298	1
Arg336		Arg336	Arg336	9
Pro337		Pro337	Pro337	9
Met339				3
			Glu340	2
		Glu342	Glu342	8
Leu345		Leu345	Leu345	6
Arg347		Gln347	Lys347	3

[a]Amino acid conservation values represent Consurf scores (9, conserved; 1, variable).

that the β-ladder might bind to the complement control protein domain (sushi domain) of complement proteins (51). In comparison, the loop face in the JEV NS1-C, with its diverse surface charges, is fully exposed compared to that of ZIKV, WNV, and DENV. In particular, DENV has the most distinct positive central area whereas the rest are negatively charged. Positively charged pockets found on the loop face of the NS1 crystal structure could mediate anionic ligand binding. Moreover, the pockets, especially pocket 1, are composed of conserved sequences and are found in all known NS1 structures. The presence or absence of each pocket in NS1 from different flaviviruses may confer upon the individual NS1 proteins the ability to interact with different target proteins or ligands in a virus-specific manner. The presence of sulfate molecules distributed on the NS1 surface agrees with previous findings for DENV and ZIKV and indicates the potential for anionic ligand interaction. We thought that NS1 might interact with uninfected cell membranes via these sulfate binding sites (32), but further experiments confirmed that JEV NS1-C cannot bind efficiently to heparin, heparan sulfate, chondroitin sulfate, or dermatan sulfate polymers. Thus, the sulfate binding sites are not GAG binding interfaces and could represent a crystallographic artifact. Moreover, JEV NS1-C cannot bind to liposomes. Our results also suggest that the NS1 C terminus is not responsible for binding to the cell membrane through GAGs. Instead, cell membrane interactions may occur at the β-roll and wing domains, as was suggested previously (22–24).

B-factor and MD analyses suggest that loop 218 to 272 is conformationally dynamic. Although the B-factor values are high for this region, the X-ray structure does not show

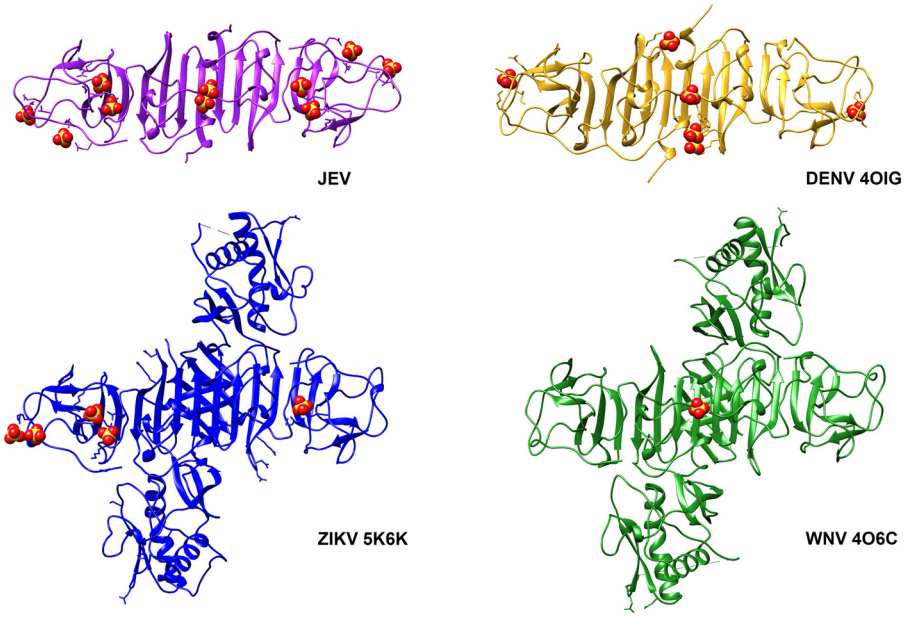

FIG 6 Sulfate molecules bound to the loop surface of JEV NS1-C. Sulfate molecules were found not only for JEV NS1 but also in DENV (PDB ID 4OIG), ZIKV (PDB ID 5K6K), and WNV (PDB ID 4O6C). Thus, it is suspected to be an importance sulfate binding interface.

disorder. Loop 218 to 272 links strands β4 and β5 and is the longest JEV NS1-C loop. Interestingly, the 22NS1 epitope forms part of this loop (Trp232, Gly235, Ile236, Leu237, Ser239, Asp240, Asn253, Try260, Lys261, and Thr262). Binding with antibody may stabilize the loop as seen in the WNV NS1-C–22NS1 complex (PDB ID 4OII). We suspect that the dynamic 218-to-272 loop may harbor distinct protein-protein interaction functions, a phenomenon which was found independently in WNV (21). NS1 from other flaviviruses may share this characteristic. Taken together, the models agree that the membrane-associated NS1 dimer orients with the N terminus facing the endoplasmic reticulum or cell membrane and the loop facing outward (21, 22, 24), making an interacting interface and likely mediating the biological functions of the protein. Therefore, the loop domain could be a candidate for structure-based drug targeting.

The 22NS1 anti-WNV NS1 MAb is protective in mice and was previously found not to cross-react with DENV-2 (36). We demonstrated that this MAb can cross-react with

TABLE 5 Sulfate contact residues from assembly analysis in the program PISA (57)

Area	C-JEV residue	ZIKV residue (5K6K)	WNV residue (4O6C)	C-DENV residue (4OIG)
Tip	Arg347	Ser342		His309
	Gln349	Glu343		Glu310
	Thr302	Thr302		Lys339
	Ser304	Ser304		
	Lys306	Arg306		
	Thr343			
	Thr344			
Positively charge pockets	Arg294	Arg294		
	Arg314	Arg261		
Central	Asp235		Gly235	His181
				Lys206
				Thr210
				Ser228
				Trp232
				Asn234
				Gly235

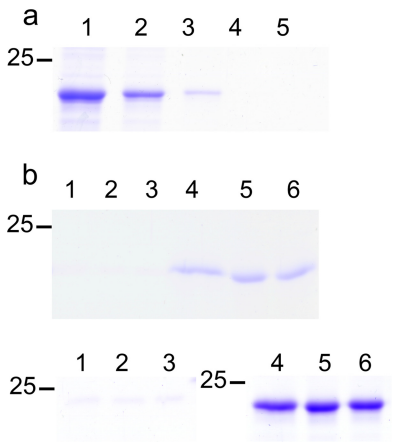

FIG 7 Cell membrane interaction via GAG determination. (a) Heparin binding determination. JEV NS1-C was incubated with heparin agarose beads. Total JEV NS1-C loaded to the column is shown in lane 1. Lane 2 shows the flowthrough fraction. Lanes 3 and 4 show wash fractions. The column was eluted with buffer supplemented with 1.5 M NaCl, and the results are shown in lane 5. Three independent experiments were conducted. (b) Liposome binding assay. The experiments were conducted at pH 7.5 (upper panel) and pH 5.5 (lower panel). Supernatant and pellet fractions separated by centrifugation were analyzed by SDS-PAGE. Lanes 1, 2, and 3 represent pellets from 400-nmol, 100-nmol, and 25-nmol reaction mixtures, respectively. Lanes 4, 5, and 6 represent supernatants from 400-nmol, 100-nmol, and 25-nmol reaction mixtures, respectively. Three independent experiments were conducted.

the more closely related JEV NS1-C at the same epitope, but with some conformational flexibility. This finding agrees with our MD result showing elasticity in the epitope loop, which may affect the antibody-NS1 structure in solution. Even though JEV NS1′-C has extra amino acids at the C terminus, JEV NS1′-C can interact with WNV 22NS1 MAb, indicating the C-terminal tail does not obstruct the binding surface of 22NS1. The C-tail may then locate at the side flanking the dimer. The presence of NS1′ is a shared characteristic of JE serocomplex viruses, and NS1′ may have specific properties that contribute to the propensity of JE serogroup viruses to cause encephalitis.

Despite flavivirus NS1 proteins having a conserved protein fold, these proteins differ

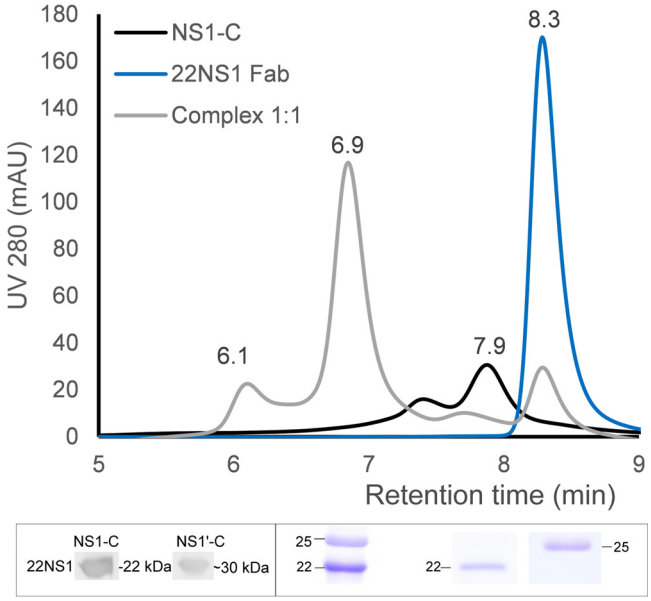

FIG 8 JEV NS1-C complexed with 22NS1 Fab. JEV NS1-C was detected by 22NS1 MAb (lower left inset). JEV NS1-C was incubated with 22NS1 Fab at 1:1 molar ratio of protein to Fab fragment, and complex formation was analyzed on an Agilent BioSEC-3 4.6/300 column. The lower right panel shows the results of SDS-PAGE analysis of each elution fraction. AU, arbitrary units.

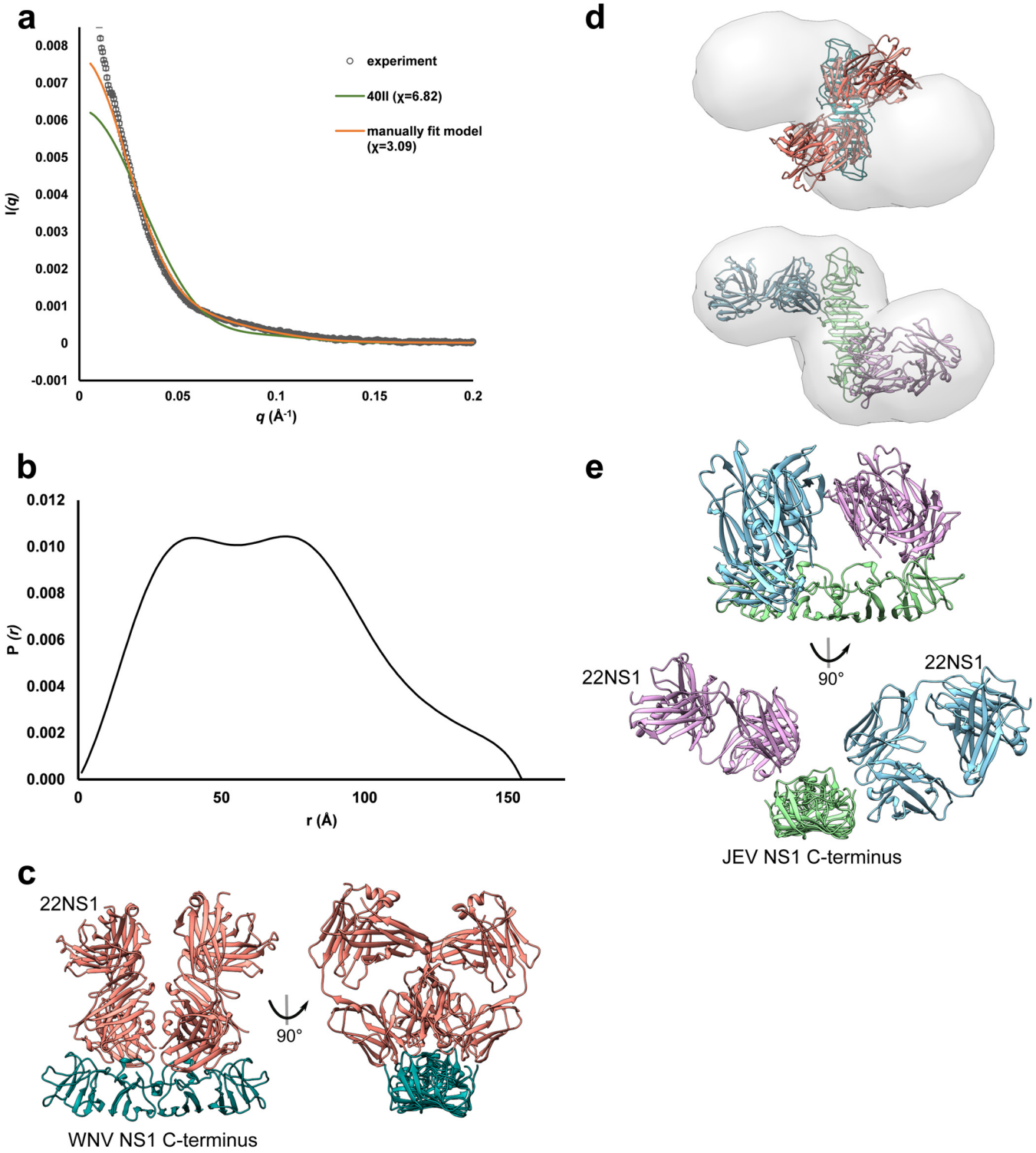

FIG 9 SAXS analysis of JEV NS1-C–22NS1 Fab complex. (a) SAXS curve. An experimental scattering curve of the JEV NS1-C–22NS1 Fab complex is shown in black scattering. The calculated scattering profile of the WNV NS1-C–22NS1 complex (PDB ID 4OII) is displayed in green, and data from the JEV NS1-C–22NS1 Fab complex manually fit model are shown in orange. (b) Pair distribution functions show multiple peaks signifying the multidomain structure. (c) WNV NS1-C–22NS1 complex (PDB ID 4OII). WNV NS1-C is colored in deep sky blue. 22NS1 Fabs are colored in salmon. (d) (Upper panel) WNV NS1-C–22NS1 complex (PDB ID 4OII) fitted to the JEV NS1-C–22NS1 Fab complex *ab initio* model. (Lower panel) A pseudoatomic model of the JEV NS1-C–22NS1 Fab complex was manually fitted to the *ab initio* model. (e) JEV NS1-C–22NS1 Fab complex pseudo-atomic model. JEV NS1-C is colored in light green. 22NS1 Fab is colored in orchid, and another Fab is colored in sky blue.

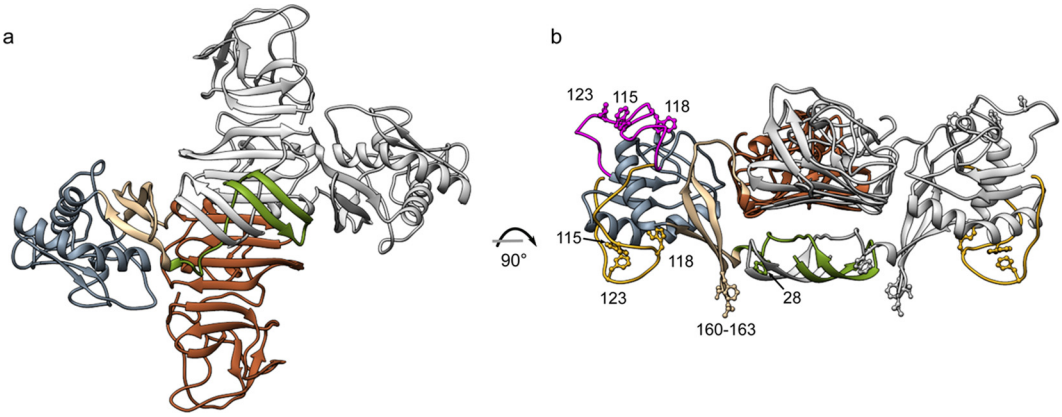

FIG 10 JEV NS1 homology model. The JEV NS1 full-length model was created by using SWISS-MODEL homology modeling. Dimerization was generated by superimposition of the JEV NS1 homology model onto ZIKV NS1 PDB ID 5GS6. (a) Cross-shaped homodimer NS1. One subunit is colored in gray, and another is colored by domain. A β-roll domain (amino acid residues 1 to 29) is colored in green, a wing domain (amino acids 38 to 151) is colored in blue, and β-ladder domains (amino acids 181 to 352) are colored in brown. (b) Side view of NS1. Residues 108 to 128 of the JEV homology model are indicated in magenta. Residues 108 to 128 are disordered and not visible in DENV (PDB ID 4O6B) or WNV (PDB ID 4O6C), but they are visible in ZIKV (PDB ID 5GS6 [shown in yellow] and 5K6K). Hydrophobic residues (namely, residues 28, 115, 118, 123, and 160 to 163) suspected to be involved with cell membrane interaction are labeled.

in their charge distributions, which may enable unique interactions with host proteins (8, 41). The fact that WNV 22NS1 MAb interacts with JEV NS1 is consistent with the high similarity of charge distributions of WNV and JEV NS1. This similarity also extends to ZIKV. Overall, these results provide structural details that aid NS1 function determination and highlight both similarities and contrasts among NS1 orthologs, which may be a productive avenue for developing common diagnostic and therapeutic strategies against diseases caused by the members of this important group of flaviviruses.

MATERIALS AND METHODS

Protein expression and refolding. JEV strain SA14 (GenBank accession no. M55506) was used as a template. Synthetic DNA optimized for expression of JEV NS1 in *E. coli* was acquired from Life Technologies. To create JEV NS1-C (amino acid residues 172 to 352), the target sequences were cloned into pET303 at XbaI/XhoI cloning sites by using forward primer 5′-gctctagaatgCGTGAAGAAAGCACCG ATGAATGTGAT-3′ and reverse primer 5′-ccgctcgagTTATGCATCAACCTGGCTACGAACCAG-3′; lowercase characters indicate the vector sequence that was required for the cloning step, and uppercase characters indicate the target sequence. Synthetic *JEV*NS1′ was purchased from GenScript (Piscataway, NJ, USA). The full-length NS1′ was the NS1 sequence with 156 additional nucleotides. The frameshift sequence was manually added by insertion of thymine at position 3561 as a result of −1 ribosomal frameshifting. JEV NS1′-C was generated from the synthetic *JEV*NS1′ by using forward primer 5′-gctctagaatg CGTGAAGAAAGCACCGATGAATGTGAT-3′ and reverse primer 5′-ccgctcgagTTAATGCAGATGATAACCC CATGCATctg-3′. Proteins were expressed in *E. coli* by autoinduction and refolded by using a method modified from that previously described by Edeling et al. (21). The theoretical molecular masses of JEV NS1-C and JEV NS1′-C are 20.54 kDa and 25.98 kDa. Protein yield and purity were analyzed by SDS-PAGE.

Protein crystallization and data collection. JEV NS1-C (~6 mg/ml) and JEV NS1′-C (5 to 7 mg/ml) were screened using commercial crystallization screens. Successful conditions were optimized by the use of the hanging drop method. Needle crystals of JEV NS1-C were produced from 1 M ammonium sulfate and 0.1 M MES [2-(*N*-morpholino)ethanesulfonic acid; pH 5.5]. The crystals were flash frozen in reservoir solution with 20% to 25% ethylene glycol added. JEV NS1′-C also crystallized in needle form in 1 M ammonium sulfate–5% propanol. JEV NS1′-C was cryo-protected in reservoir solution–20% glycerol.

X-ray data were collected at cryogenic temperature, at a wavelength of 0.98 Å, at beamline PROXIMA 1 at the Soleil synchrotron (France) and at beamline I02 at the Diamond Light Source (United Kingdom). Data reduction was carried out by the use of XDS programs (52) or iMOSFLM (53). The protein structure was determined by molecular replacement using the structure of the WNV NS1 C-terminal domain (PDB ID 4OII; sequence identity, >70%) as a starting model by the use of MOLREP (54) in the CCP4 program suite. The structure was refined by the use of REFMAC5 (55) and built in COOT (56). Data collection and refinement statistics are shown in Table 6. The JEV NS1-C refinement statistic values from a Ramachandran plot are 95.98% favored and 0% outliers. The MolProbity score is 1.6. The JEV NS1′-C refinement statistic values from a Ramachandran plot are 94.89% favored and 0% outliers. The MolProbity score is 1.84.

Protein structure analysis. Assembly analysis was performed by the use of the program PISA (57). Conservation scores of residues on protein structures were determined by the use of ConSurf (58) with

TABLE 6 Data collection and refinement statistics

Parameter	Value(s)[b]	
	JEV NS1-C	JEV NS1′-C
Data collection		
Space group	I212121	I212121
Cell dimensions		
a, *b*, *c* (Å)	49.42, 78.24, 163.18	50.32, 77.94, 163.49
a, b, g (°)	90, 90, 90	90, 90, 90
Resolution (Å)	47.3–2.10 (2.21–2.10)	81.75–2.6 (2.72–2.6)
R_{merge}	0.103 (0.907)	0.2 (1.413)
R_{pim}	0.045 (0.383)	0.141 (1.030)
$I/\sigma I$	11.5 (2.3)	7.1 (2.1)
Completeness (%)	99.8 (99.6)	99.9 (99.9)
Redundancy	6.3 (6.5)	5.3 (5.2)
Refinement		
Resolution (Å)	47.3–2.10	81.75–2.6
No. of reflections	17,944	9719
R_{work}/R_{free}	0.189/0.228	0.166/0.225
No. of atoms	1574	1573
Protein	1398	1418
Sulfate ion	60	60
Ligand	24 (MES)	4 (POL[a])
Water	92	91
B-factors		
Protein	41.516	38.612
Sulfate ion	90.121	85.148
Ligand	86.736 (MES)	61.722 (POL)
Water	50.187	48.669
RMS deviations		
Bond lengths (Å)	0.016	0.016
Bond angles (°)	1.785	1.741

[a]POL, *n*-propanol.
[b]Values in parentheses are for the highest-resolution shell.

21 homologous sequences. The input homologous sequences of NS1 C terminus were searched by the program, and existing NS1 structure sequences were added manually. Electrostatic surface maps were generated by using PDB2PQR (59) to convert PDB files into PQR files and Adaptive Poisson-Boltzmann Solver (APBS) for electrostatics calculations (60) without pK_a prediction.

JEV NS1 C terminus-22NS1 complex formation. Complex formation was confirmed by Western blotting, with 22NS1 (36) and goat anti-mouse IgG-horseradish peroxidase (IgG-HRP; Santa Cruz Biotechnology, sc-2055) used as primary and secondary antibodies, respectively. Purified JEV NS1 C terminus and 22NS1 fragment antigen binding (Fab) (prepared from 22NS1 IgG MAb using a Pierce Fab Preparation kit; catalog no. 44985) were mixed overnight at 4°C at a 1:1 ratio of JEV NS1-C to 22NS1 and purified by the use of Agilent Bio SEC-3 4.6 300 or GE Superdex 200 10 300 GL. Eluted fractions were analyzed by SDS-PAGE.

SAXS data collection and processing. JEV NS1-C at a concentration of 3.4 mg/ml and JEV NS1-C–22NS1 Fab complex at concentration of 3 mg/ml in TBS buffer (20 mM Tris-HCl [pH 7.4], 150 mM NaCl) were analyzed with SEC-SAXS on beamline SWING at the Soleil synchrotron (France). Samples were loaded onto an Agilent BioSEC-3 4.6/300 column at a flow rate of 0.25 ml/min at 15°C. Data were collected at a distance of 1.8 m and an X-ray wavelength of 1 Å. Data processing was conducted in PRIMUS (61). Comparison of scattering profiles was done in FoXS (62). The *ab initio* model included averages from 10 (JEV NS1-C) or 20 (protein complex) independent model calculations with symmetry (protein complex) or without symmetry (JEV NS1-C) determined using DAMMIF (63). The model data were averaged with DAMAVER (64) and refined with DAMMIN (65). The low-resolution-model surface representation was created in CHIMERA (66) using the 'molmap' command. The molecular mass was calculated from Porod volume data (67). Molecular dynamics (MD) simulations were performed using GROMACS 4.6.5 and GROMOS96 54A7 force fields in a cubic box solvated with single-point charge-E water molecules on JEV NS1-C dimers. A neutral charge was introduced at 150 mM NaCl. The distance between the JEV NS1-C dimers and the box edge was set to 10 Å. Long-range interactions were defined using the particle mesh Ewald algorithm, and other nonbonded interactions were restricted to 10 Å. An energy minimization step was performed using the steepest descent algorithm followed by a 100-ps NVT ensemble at 310 K and a 200-ps NPT ensemble at 310 K and 10^5 Pa. Production MD analyses were performed at 310 K and 10^5 Pa for 40 ns. Cα displacement was calculated with the GROMACS root mean square fluctuation (RMSF) function. Torsion angle MD analyses were performed with CNS software at 100,000 K for 37.5 ps with sampling performed every 7.5 fs in eight separate simulations. The best structure was found with FoXS using experimental data over a data range of $0.017 < q < 0.25$ Å^{-1}, where

$q = (4\pi \sin \theta)/\lambda$, 2θ is the angle between the incident X-ray beam and the detector measuring the scattered intensity, and λ is the wavelength of the X-rays, and was refined with another eight separate 7.5-ps simulations and energy minimization in GROMACS using the procedure described above. The models were compared again using FoXS. Freeing loop 214 to 243 gave a value of 1.66 corresponding to the fit with experimental data. Expanding the flexible region to 218 to 272 allowed us to improve the fit to 1.48.

Liposome binding assay. The liposome preparation method was modified from methods described in previous publications (49, 68). Liposomes were prepared from cholesterol (CHOL) (Sigma, C8667) and 1,2-dipalmitoyl-sn-glycero-3-phosphocholine (PC) (Sigma, P4329) at a 1:9 ratio of CHOL to PC (22, 49, 68). CHOL and PC powders were dissolved in chloroform. To achieve a total of 400 nmol, 40 nmol of CHOL and 360 nmol of PC were mixed together in a 2-ml tube, and the lipid mixture was dried under a nitrogen gas stream. To hydrate the lipid sheets, 50 μl of buffer consisting of 50 mM Bis-Tris (pH 5.5), 50 mM $(NH_4)_2S0_4$, and 10% glycerol or 150 mM KCl, 25 mM Tris-HCl (pH 7.5), 1 mM dithiothreitol (DTT), and 0.5 mM (EDTA) was added and the reaction mixture was incubated at room temperature on a shaker for 30 min. Then, the lipid was sonicated with an exponential probe at amplitude 4 for 30 s with a 30-s interval on a warmed water bath for 5 times. A liposome binding reaction (50 μl) was set up using 400 nmol, 125 nmol, and 25 nmol of total lipid, and the reaction mixture was then mixed with 5 μg of protein. The reaction mixtures were incubated at 37°C for 45 min. After that, the reactions were centrifuged at 16,000 $\times$ *g* for 30 min at 22°C and the supernatant was transferred to a new tube. The lipid pellet was resuspended in 200 μl buffer and also transferred to a new tube. Liposomes were pelleted again, and the supernatant was discarded. The liposome pellet was resuspended in 30 μl of 1$\times$ SDS-PAGE sample buffer. Bovine cytochrome bc1 complex (membrane proteins) was used as the positive control in a mixture consisting of 25 mM phosphate buffer (pH 7.5), 100 mM NaCl, 3 mM NaN_3, and 0.015% DDM (*n*-dodecyl-D-maltoside) buffer. The supernatant and pellet fractions were analyzed by SDS-PAGE.

Heparin binding assay. A small-scale 50-μl column was set up using a pipette tip and heparin agarose beads (Affi-Gel heparin gel; Bio-Rad). The binding buffer was 20 mM HEPES (pH 7.4) supplemented with 150 mM NaCl, and the elution buffer was 20 mM HEPES (pH 7.4) supplemented with 1.5 M and 2 M NaCl. The column was equilibrated with 400 μl of binding buffer. JEV NS1-C (5 μg) was applied to the column, and the column was incubated on a roller for 30 min at 4°C. The column was washed 3 times with 400 μl binding buffer before elution was performed twice with 100 μl of 1.5 M and 2 M NaCl elution buffer. Superoxide dismutase 3 (SOD3), which contains a heparin binding domain, was used as a positive control. Samples from each step (including the loading, flowthrough, washing, and elution steps) were analyzed by SDS-PAGE.

Differential scanning fluorimetry (DSF). Polymers of heparan sulfate (average molecular weight, 30,000), chondroitin sulfate (62% chondroitin 4-sulfate and 33% chondroitin 6-sulfate; average molecular weight, 45,400), and dermatan sulfate (average molecular weight, 41,000) (Iduron) at final concentrations of 100, 50, 25, 10, 5, 1, and 0.5 μM were mixed with JEV NS1-C and Sypro Orange 5000X (Invitrogen) at final concentrations of 10 μM and 10$\times$, respectively. The reaction volume was 10 μl. The experiments were set up in 96-well plates and performed using StepOnePlus Real-Time PCR Systems (software version 2.3) (Applied Biosystems). The reactions were equilibrated at 25°C for 2 min followed by an increase to 95°C at 1°C min^{-1}. The experiments were performed in three replicates.

Data availability. The atomic coordinates and structure factors have been deposited in the Protein Data Bank (www.pdb.org) (PDB ID 5O19 for JEV NS1-C and 5O36 for JEV NS1′-C).

ACKNOWLEDGMENTS

This work was supported by a Mahidol-Liverpool Stang Mongkolsuk Ph.D. scholarship. We acknowledge help from the following colleagues at the University of Liverpool: Richard Strange for assistance with the electrostatic surface map; Sujitra Keadsanti for assistance with Western blotting; Kangsa Amporndanai for providing bovine cytochrome *bc1*; Varunya Chantadul for providing human SOD3; and Pawin Ngamlert for assistance with the heparin binding assay. We also thank Samar Hasnain for support and interest in the project throughout and for extensive discussions of the results. We acknowledge Synchrotron Soleil for provision of the Proxima 1 beamline and SAXS facilities.

Use of Soleil was funded by the European Community's Seventh Framework Programme (FP7/2007-2013) under BioStruct-X (grant agreement number 283570 and proposal number 6714). We gratefully acknowledge the Diamond Synchrotron for providing support at the I02 beamline. M.S.D. acknowledges support from HHSN272201400018C, L.T. from The Wellcome Trust (grant number 205228/Z/16/Z), and T.S. and L.T. from the National Institute for Health Research (NIHR; www.nihr.ac.uk) Health Protection Research Unit in Emerging and Zoonotic Infections.

T.S. and S.V.A. originated and designed the project; T.P. expressed and purified proteins; T.P. and G.S.A.W. performed the experiments; T.P., G.S.A.W., and S.V.A. undertook data analysis; and T.P., G.S.A.W., M.S.D., T.S., L.T., and S.V.A. contributed to interpretation of data and wrote the manuscript.

REFERENCES

1. Lindenbach BD, Rice CM. 1997. trans-Complementation of yellow fever virus NS1 reveals a role in early RNA replication. J Virol 71:9608–9617.
2. Mackenzie JM, Jones MK, Young PR. 1996. Immunolocalization of the dengue virus nonstructural glycoprotein NS1 suggests a role in viral RNA replication. Virology 220:232–240. https://doi.org/10.1006/viro.1996.0307.
3. Muylaert IR, Chambers TJ, Galler R, Rice CM. 1996. Mutagenesis of the N-linked glycosylation sites of the yellow fever virus NS1 protein: effects on virus replication and mouse neurovirulence. Virology 222:159–168. https://doi.org/10.1006/viro.1996.0406.
4. Youn S, Ambrose RL, Mackenzie JM, Diamond MS. 2013. Non-structural protein-1 is required for West Nile virus replication complex formation and viral RNA synthesis. Virol J 10:339. https://doi.org/10.1186/1743-422X-10-339.
5. Fan J, Liu Y, Yuan Z. 2014. Critical role of dengue virus NS1 protein in viral replication. Virol Sin 29:162–169. https://doi.org/10.1007/s12250-014-3459-1.
6. Lindenbach BD, Rice CM. 1999. Genetic interaction of flavivirus nonstructural proteins NS1 and NS4A as a determinant of replicase function. J Virol 73:4611–4621.
7. Youn S, Li T, McCune BT, Edeling MA, Fremont DH, Cristea IM, Diamond MS. 2012. Evidence for a genetic and physical interaction between nonstructural proteins NS1 and NS4B that modulates replication of West Nile virus. J Virol 86:7360–7371. https://doi.org/10.1128/JVI.00157-12.
8. Krishna VD, Rangappa M, Satchidanandam V. 2009. Virus-specific cytolytic antibodies to nonstructural protein 1 of Japanese encephalitis virus effect reduction of virus output from infected cells. J Virol 83:4766–4777. https://doi.org/10.1128/JVI.01850-08.
9. Winkler G, Randolph VB, Cleaves GR, Ryan TE, Stollar V. 1988. Evidence that the mature form of the flavivirus nonstructural protein NS1 is a dimer. Virology 162:187–196. https://doi.org/10.1016/0042-6822(88)90408-4.
10. Schlesinger JJ, Brandriss MW, Putnak JR, Walsh EE. 1990. Cell surface expression of yellow fever virus non-structural glycoprotein NS1: consequences of interaction with antibody. J Gen Virol 71(Pt 3):593–599. https://doi.org/10.1099/0022-1317-71-3-593.
11. Lee JM, Crooks AJ, Stephenson JR. 1989. The synthesis and maturation of a non-structural extracellular antigen from tick-borne encephalitis virus and its relationship to the intracellular NS1 protein. J Gen Virol 70(Pt 2):335–343. https://doi.org/10.1099/0022-1317-70-2-335.
12. Avirutnan P, Hauhart RE, Somnuke P, Blom AM, Diamond MS, Atkinson JP. 2011. Binding of flavivirus nonstructural protein NS1 to C4b binding protein modulates complement activation. J Immunol 187:424–433. https://doi.org/10.4049/jimmunol.1100750.
13. Avirutnan P, Fuchs A, Hauhart RE, Somnuke P, Youn S, Diamond MS, Atkinson JP. 2010. Antagonism of the complement component C4 by flavivirus nonstructural protein NS1. J Exp Med 207:793–806. https://doi.org/10.1084/jem.20092545.
14. Chung KM, Liszewski MK, Nybakken G, Davis AE, Townsend RR, Fremont DH, Atkinson JP, Diamond MS. 2006. West Nile virus nonstructural protein NS1 inhibits complement activation by binding the regulatory protein factor H. Proc Natl Acad Sci U S A 103:19111–19116. https://doi.org/10.1073/pnas.0605668103.
15. Morrison CR, Scholle F. 2014. Abrogation of TLR3 inhibition by discrete amino acid changes in the C-terminal half of the West Nile virus NS1 protein. Virology 456–457:96–107.
16. Glasner DR, Ratnasiri K, Puerta-Guardo H, Espinosa DA, Beatty PR, Harris E. 2017. Dengue virus NS1 cytokine-independent vascular leak is dependent on endothelial glycocalyx components. PLoS Pathog 13:e1006673. https://doi.org/10.1371/journal.ppat.1006673.
17. Modhiran N, Watterson D, Blumenthal A, Baxter AG, Young PR, Stacey KJ. 21 February 2017. Dengue virus NS1 protein activates immune cells via TLR4 but not TLR2 or TLR6. Immunol Cell Biol https://doi.org/10.1038/icb.2017.5.
18. Modhiran N, Watterson D, Muller DA, Panetta AK, Sester DP, Liu L, Hume DA, Stacey KJ, Young PR. 2015. Dengue virus NS1 protein activates cells via Toll-like receptor 4 and disrupts endothelial cell monolayer integrity. Sci Transl Med 7:304ra142. https://doi.org/10.1126/scitranslmed.aaa3863.
19. Han YW, Choi JY, Uyangaa E, Kim SB, Kim JH, Kim BS, Kim K, Eo SK. 2014. Distinct dictation of Japanese encephalitis virus-induced neuroinflammation and lethality via triggering TLR3 and TLR4 signal pathways. PLoS Pathog 10:e1004319. https://doi.org/10.1371/journal.ppat.1004319.
20. Muller DA, Young PR. 2013. The flavivirus NS1 protein: molecular and structural biology, immunology, role in pathogenesis and application as a diagnostic biomarker. Antiviral Res 98:192–208. https://doi.org/10.1016/j.antiviral.2013.03.008.
21. Edeling MA, Diamond MS, Fremont DH. 2014. Structural basis of flavivirus NS1 assembly and antibody recognition. Proc Natl Acad Sci U S A 111:4285–4290. https://doi.org/10.1073/pnas.1322036111.
22. Akey DL, Brown WC, Dutta S, Konwerski J, Jose J, Jurkiw TJ, DelProposto J, Ogata CM, Skiniotis G, Kuhn RJ, Smith JL. 2014. Flavivirus NS1 structures reveal surfaces for associations with membranes and the immune system. Science 343:881–885. https://doi.org/10.1126/science.1247749.
23. Xu X, Song H, Qi J, Liu Y, Wang H, Su C, Shi Y, Gao GF. 30 August 2016. Contribution of intertwined loop to membrane association revealed by Zika virus full-length NS1 structure. EMBO J https://doi.org/10.15252/embj.201695290.
24. Brown WC, Akey DL, Konwerski JR, Tarrasch JT, Skiniotis G, Kuhn RJ, Smith JL. 2016. Extended surface for membrane association in Zika virus NS1 structure. Nat Struct Mol Biol 23:865–867. https://doi.org/10.1038/nsmb.3268.
25. Blitvich BJ, Scanlon D, Shiell BJ, Mackenzie JS, Pham K, Hall RA. 2001. Determination of the intramolecular disulfide bond arrangement and biochemical identification of the glycosylation sites of the nonstructural protein NS1 of Murray Valley encephalitis virus. J Gen Virol 82:2251–2256. https://doi.org/10.1099/0022-1317-82-9-2251.
26. Mandl CW, Heinz FX, Stockl E, Kunz C. 1989. Genome sequence of tick-borne encephalitis virus (Western subtype) and comparative analysis of nonstructural proteins with other flaviviruses. Virology 173:291–301. https://doi.org/10.1016/0042-6822(89)90246-8.
27. Watterson D, Modhiran N, Young PR. 2016. The many faces of the flavivirus NS1 protein offer a multitude of options for inhibitor design. Antiviral Res 130:7–18. https://doi.org/10.1016/j.antiviral.2016.02.014.
28. Gutsche I, Coulibaly F, Voss JE, Salmon J, d'Alayer J, Ermonval M, Larquet E, Charneau P, Krey T, Megret F, Guittet E, Rey FA, Flamand M. 2011. Secreted dengue virus nonstructural protein NS1 is an atypical barrel-shaped high-density lipoprotein. Proc Natl Acad Sci U S A 108:8003–8008. https://doi.org/10.1073/pnas.1017338108.
29. Jacobs MG, Robinson PJ, Bletchly C, Mackenzie JM, Young PR. 2000. Dengue virus nonstructural protein 1 is expressed in a glycosyl-phosphatidylinositol-linked form that is capable of signal transduction. FASEB J 14:1603–1610. https://doi.org/10.1096/fj.99-0829com.
30. Noisakran S, Dechtawewat T, Avirutnan P, Kinoshita T, Siripanyaphinyo U, Puttikhunt C, Kasinrerk W, Malasit P, Sittisombut N. 2008. Association of dengue virus NS1 protein with lipid rafts. J Gen Virol 89:2492–2500. https://doi.org/10.1099/vir.0.83620-0.
31. Noisakran S, Dechtawewat T, Rinkaewkan P, Puttikhunt C, Kanjanahaluethai A, Kasinrerk W, Sittisombut N, Malasit P. 2007. Characterization of dengue virus NS1 stably expressed in 293T cell lines. J Virol Methods 142:67–80. https://doi.org/10.1016/j.jviromet.2007.01.008.
32. Avirutnan P, Zhang L, Punyadee N, Manuyakorn A, Puttikhunt C, Kasinrerk W, Malasit P, Atkinson JP, Diamond MS. 2007. Secreted NS1 of dengue virus attaches to the surface of cells via interactions with heparan sulfate and chondroitin sulfate E. PLoS Pathog 3:e183. https://doi.org/10.1371/journal.ppat.0030183.
33. Li YZ, Counor D, Lu P, Liang GD, Vu TQ, Phan TN, Huynh TK, Sun G, Grandadam M, Butrapet S, Lavergne JP, Flamand M, Yu YX, Solomon T, Buchy P, Deubel V. 2012. A specific and sensitive antigen capture assay for NS1 protein quantitation in Japanese encephalitis virus infection. J Virol Methods 179:8–16. https://doi.org/10.1016/j.jviromet.2011.06.008.
34. Amorim JH, Alves RP, Boscardin SB, Ferreira LC. 2014. The dengue virus non-structural 1 protein: risks and benefits. Virus Res 181:53–60. https://doi.org/10.1016/j.virusres.2014.01.001.
35. Solomon T, Thao LT, Dung NM, Kneen R, Hung NT, Nisalak A, Vaughn DW, Farrar J, Hien TT, White NJ, Cardosa MJ. 1998. Rapid diagnosis of Japanese encephalitis by using an immunoglobulin M dot enzyme immunoassay. J Clin Microbiol 36:2030–2034.
36. Chung KM, Nybakken GE, Thompson BS, Engle MJ, Marri A, Fremont DH, Diamond MS. 2006. Antibodies against West Nile virus nonstructural protein NS1 prevent lethal infection through Fc gamma receptor-dependent and -independent mechanisms. J Virol 80:1340–1351. https://doi.org/10.1128/JVI.80.3.1340-1351.2006.
37. Schlesinger JJ, Brandriss MW, Cropp CB, Monath TP. 1986. Protection

against yellow fever in monkeys by immunization with yellow fever virus nonstructural protein NS1. J Virol 60:1153–1155.
38. Schlesinger JJ, Foltzer M, Chapman S. 1993. The Fc portion of antibody to yellow fever virus NS1 is a determinant of protection against YF encephalitis in mice. Virology 192:132–141. https://doi.org/10.1006/viro.1993.1015.
39. Li Y, Counor D, Lu P, Duong V, Yu Y, Deubel V. 2012. Protective immunity to Japanese encephalitis virus associated with anti-NS1 antibodies in a mouse model. Virol J 9:135. https://doi.org/10.1186/1743-422X-9-135.
40. Liu J, Liu Y, Nie K, Du S, Qiu J, Pang X, Wang P, Cheng G. 2016. Flavivirus NS1 protein in infected host sera enhances viral acquisition by mosquitoes. Nat Microbiol 1:16087. https://doi.org/10.1038/nmicrobiol.2016.87.
41. Cheng HJ, Lin CF, Lei HY, Liu HS, Yeh TM, Luo YH, Lin YS. 2009. Proteomic analysis of endothelial cell autoantigens recognized by anti-dengue virus nonstructural protein 1 antibodies. Exp Biol Med (Maywood) 234:63–73. https://doi.org/10.3181/0805-RM-147.
42. Beatty PR, Puerta-Guardo H, Killingbeck SS, Glasner DR, Hopkins K, Harris E. 2015. Dengue virus NS1 triggers endothelial permeability and vascular leak that is prevented by NS1 vaccination. Sci Transl Med 7:304ra141. https://doi.org/10.1126/scitranslmed.aaa3787.
43. Melian EB, Hinzman E, Nagasaki T, Firth AE, Wills NM, Nouwens AS, Blitvich BJ, Leung J, Funk A, Atkins JF, Hall R, Khromykh AA. 2010. NS1′ of flaviviruses in the Japanese encephalitis virus serogroup is a product of ribosomal frameshifting and plays a role in viral neuroinvasiveness. J Virol 84:1641–1647. https://doi.org/10.1128/JVI.01979-09.
44. Mason PW. 1989. Maturation of Japanese encephalitis virus glycoproteins produced by infected mammalian and mosquito cells. Virology 169:354–364. https://doi.org/10.1016/0042-6822(89)90161-X.
45. Young LB, Melian EB, Khromykh AA. 2013. NS1′ colocalizes with NS1 and can substitute for NS1 in West Nile virus replication. J Virol 87:9384–9390. https://doi.org/10.1128/JVI.01101-13.
46. Ye Q, Li XF, Zhao H, Li SH, Deng YQ, Cao RY, Song KY, Wang HJ, Hua RH, Yu YX, Zhou X, Qin ED, Qin CF. 2012. A single nucleotide mutation in NS2A of Japanese encephalitis-live vaccine virus (SA14-14-2) ablates NS1′ formation and contributes to attenuation. J Gen Virol 93:1959–1964. https://doi.org/10.1099/vir.0.043844-0.
47. Melian EB, Hall-Mendelin S, Du F, Owens N, Bosco-Lauth AM, Nagasaki T, Rudd S, Brault AC, Bowen RA, Hall RA, van den Hurk AF, Khromykh AA. 2014. Programmed ribosomal frameshift alters expression of West Nile virus genes and facilitates virus replication in birds and mosquitoes. PLoS Pathog 10:e1004447. https://doi.org/10.1371/journal.ppat.1004447.
48. Takamatsu Y, Okamoto K, Dinh DT, Yu F, Hayasaka D, Uchida L, Nabeshima T, Buerano CC, Morita K. 2014. NS1′ protein expression facilitates production of Japanese encephalitis virus in avian cells and embryonated chicken eggs. J Gen Virol 95:373–383. https://doi.org/10.1099/vir.0.057968-0.
49. Smith JL, Akey DL, Brown WC, Kuhn RJ. June 2015. Vaccine compositions and uses thereof.US patent WO 2015095735 A2.
50. Song H, Qi J, Haywood J, Shi Y, Gao GF. 2016. Zika virus NS1 structure reveals diversity of electrostatic surfaces among flaviviruses. Nat Struct Mol Biol 23:456–458. https://doi.org/10.1038/nsmb.3213.
51. Akey DL, Brown WC, Jose J, Kuhn RJ, Smith JL. 2015. Structure-guided insights on the role of NS1 in flavivirus infection. Bioessays 37:489–494. https://doi.org/10.1002/bies.201400182.
52. Kabsch W. 2010. XDS. Acta Crystallogr D Biol Crystallogr 66:125–132. https://doi.org/10.1107/S0907444909047337.
53. Battye TG, Kontogiannis L, Johnson O, Powell HR, Leslie AG. 2011. iMOSFLM: a new graphical interface for diffraction-image processing with MOSFLM. Acta Crystallogr D Biol Crystallogr 67:271–281. https://doi.org/10.1107/S0907444910048675.
54. Vagin A, Teplyakov A. 2010. Molecular replacement with MOLREP. Acta Crystallogr D Biol Crystallogr 66:22–25. https://doi.org/10.1107/S0907444909042589.
55. Murshudov GN, Skubak P, Lebedev AA, Pannu NS, Steiner RA, Nicholls RA, Winn MD, Long F, Vagin AA. 2011. REFMAC5 for the refinement of macromolecular crystal structures. Acta Crystallogr D Biol Crystallogr 67:355–367. https://doi.org/10.1107/S0907444911001314.
56. Emsley P, Lohkamp B, Scott WG, Cowtan K. 2010. Features and development of Coot. Acta Crystallogr D Biol Crystallogr 66:486–501. https://doi.org/10.1107/S0907444910007493.
57. Krissinel E, Henrick K. 2007. Inference of macromolecular assemblies from crystalline state. J Mol Biol 372:774–797. https://doi.org/10.1016/j.jmb.2007.05.022.
58. Landau M, Mayrose I, Rosenberg Y, Glaser F, Martz E, Pupko T, Ben-Tal N. 2005. ConSurf 2005: the projection of evolutionary conservation scores of residues on protein structures. Nucleic Acids Res 33:W299–W302. https://doi.org/10.1093/nar/gki370.
59. Dolinsky TJ, Czodrowski P, Li H, Nielsen JE, Jensen JH, Klebe G, Baker NA. 2007. PDB2PQR: expanding and upgrading automated preparation of biomolecular structures for molecular simulations. Nucleic Acids Res 35:W522–W525. https://doi.org/10.1093/nar/gkm276.
60. Baker NA, Sept D, Joseph S, Holst MJ, McCammon JA. 2001. Electrostatics of nanosystems: application to microtubules and the ribosome. Proc Natl Acad Sci U S A 98:10037–10041. https://doi.org/10.1073/pnas.181342398.
61. Konarev PV, Volkov VV, Sokolova AV, Koch MHJ, Svergun DI. 2003. PRIMUS: a Windows PC-based system for small-angle scattering data analysis. J Appl Crystallogr 36:1277–1282. https://doi.org/10.1107/S0021889803012779.
62. Schneidman-Duhovny D, Hammel M, Tainer JA, Sali A. 2013. Accurate SAXS profile computation and its assessment by contrast variation experiments. Biophys J 105:962–974. https://doi.org/10.1016/j.bpj.2013.07.020.
63. Franke D, Svergun DI. 2009. DAMMIF, a program for rapid ab-initio shape determination in small-angle scattering. J Appl Crystallogr 42:342–346. https://doi.org/10.1107/S0021889809000338.
64. Volkov VV, Svergun DI. 2003. Uniqueness of ab initio shape determination in small-angle scattering. J Appl Crystallogr 36:860–864. https://doi.org/10.1107/S0021889803000268.
65. Svergun DI. 1999. Restoring low resolution structure of biological macromolecules from solution scattering using simulated annealing. Biophys J 76:2879–2886. https://doi.org/10.1016/S0006-3495(99)77443-6.
66. Pettersen EF, Goddard TD, Huang CC, Couch GS, Greenblatt DM, Meng EC, Ferrin TE. 2004. UCSF Chimera–a visualization system for exploratory research and analysis. J Comput Chem 25:1605–1612. https://doi.org/10.1002/jcc.20084.
67. Petoukhov MV, Franke D, Shkumatov AV, Tria G, Kikhney AG, Gajda M, Gorba C, Mertens HDT, Konarev PV, Svergun DI. 2012. New developments in the ATSAS program package for small-angle scattering data analysis. J Appl Crystallogr 45:342–350. https://doi.org/10.1107/S0021889812007662.
68. Julkowska MM, Rankenberg JM, Testerink C. 2013. Liposome-binding assays to assess specificity and affinity of phospholipid-protein interactions. Methods Mol Biol 1009:261–271. https://doi.org/10.1007/978-1-62703-401-2_24.